Finite Element Implementation of a Novel Version of Strain Gradient Elasticity

M. LEDERER and G. KHATIBI
Institute of Chemical Technologies and Analytics
Vienna University of Technology
Getreidemarkt 9, 1060 Wien
AUSTRIA
martin.lederer@tuwien.ac.at golta.khatibi@tuwien.ac.at

Abstract: A novel version of strain gradient elasticity is proposed. This theory emerges from an older version of strain gradient elasticity suggested by Toupin and Mindlin through replacement of their asymmetric stress by a symmetric stress tensor. In this way one derives an improvement of the theory which is mathematically sound. Since analytical solutions are not easy to achieve within this approach, a numerical solution is elaborated with use of Finite Element Analysis. Thus, the theory is implemented in the commercial FEM software ABAQUS through user subroutine UEL. It is demonstrated for the example of a shear test that the stress singularities occurring in classical continuum theory have now disappeared.

Key-Words: Finite Element Analysis, Strain Gradient Elasticity, shear test, singularity removal

1 Introduction

In recent years strain gradient theory has attracted the interest of numerous scientist for two main reasons: First, strain gradient theory usually reduces the value of stress concentrations which sometimes appear exaggerated within classical continuum mechanics. And second, it predicts a size effect in the sense smaller is stronger. These results were confirmed experimentally on many occasions. Nevertheless, some scientists still have doubt about the soundness of this theory, because some details were never proved mathematically. Let us therefore get back to the fundamental aspects of strain gradient elasticity as they were proposed in an early publication of Mindlin [1]. Following the principles of Cosserat theory [2], an asymmetric stress tensor was assumed where the shear stresses τ_{xy} and τ_{yx} are not equal. The torque arising from the asymmetric shears in static equilibrium was compensated by couple stresses μ_x and μ_y corresponding to bending moments [1]:

$$\frac{\partial \mu_x}{\partial x} + \frac{\partial \mu_y}{\partial y} + \tau_{xy} - \tau_{yx} = 0 \qquad (1)$$

Further, the bending moments were correlated to a bending stiffness described by a bending modulus B. Consequently, the bending stiffness arising from the microstructure of a crystal [3] was considered as a correction to Hooke's law. This lead to the constitutive equation (1), where the couple stresses μ were related to the curvature of the crystal lattice. With use of a compatibility condition it was shown that the curvatures are equivalent to linear combinations of strain gradients. In this way a linear theory was obtained where strain gradients were related to couple stresses similar as strains are related to ordinary stresses.

However, the approach described by equation (1) includes a serious flaw: Couple stresses are components of a tensor which has a rank higher than two. In conclusion, the torque arising from an asymmetric stress tensor cannot consequently be compensated by the torque associated with a tensor of higher rank. In fact, there are different transformation rules for tensors of different rank during rotation of a coordinate system. Therefore, couple stress theory does not consequently fulfill the requirement of invariance with respect to rotation of the coordinate system.

In spite of this deficiency, strain gradient theory still contains important aspects which are correct. In particular, the density of elastic energy may be described by

$$w = \frac{1}{2}\left(\sigma_{ij} \cdot \varepsilon_{ij} + \mu_{ijk} \cdot \eta_{ijk}\right), \qquad (2)$$

where summation is carried out over repeated indices. Here, the μ_{ijk} are called higher order stresses and η_{ijk} are the strain gradients $\partial^2 u_i/\partial x_j \partial x_k$, where u_i are the displacements and x_i are the coordinates. In the most general two-dimensional isotropic case, the

energy density associated with the strain gradients may also be expressed as [3,4]

$$w^{sg} = \frac{1}{2}(B_1\eta_{ijk}\eta_{ijk} + B_2\eta_{ijj}\eta_{ikk} + B_3\eta_{iik}\eta_{kjj} + B_4\eta_{iik}\eta_{jjk} + B_5\eta_{ijk}\eta_{jki}), \quad (3)$$

where summation is again carried out over repeated indices. Here, B_1 through B_5 are components of the bending tensor. In this context, equation (3) represents the most general expression which is invariant with respect to rotation of the coordinate system. In contrast to Toupin [5, 6], Mindlin and others [3, 7-11], however, σ_{ij} of equation (2) is interpreted as symmetric tensor throughout the present study. In consequence, equation (1) is omitted hereafter.

The modification suggested here has some important consequences: After equation (1) is eliminated, it gets very difficult to find any analytical solutions. On the other hand, the new theory may be solved numerically using the algorithms of Finite Element Analysis. In this way one derives a linear elastic global stiffness matrix K. The relation between nodal forces F and nodal displacements U takes the simple form $F = K \cdot U$, where K is symmetric. It should be said here that the validity of the present approach is restricted to small deformations.

2 Finite Element Implementation

The elements defined in the following subsection are rectangular quadrilaterals. At first sight the restriction to rectangular elements seems to be a disadvantage compared to arbitrary element shapes. Nevertheless, these elements may be applied to a wide class of problems discussed in engineering fracture mechanics. Moreover, the rectangular elements facilitate the assessment whether convergence is achieved during mesh refinement. Hence, our interest is focused on the simplest elements which are adequate to implement the constitutive equations (2) and (3).

But at first elements of Shu et al. [4] and Zybell et al. [12] are reexamined briefly. These elements were based on the Toupin-Mindlin approach. It follows immediately that their method of using an asymmetric stress tensor is different from the assumptions of the present study. But aside from this detail it is interesting to look how these authors derived the C^1 continuity at element boundaries which is necessary for strain gradient theories. When discontinuous jumps of strain were appearing at element boundaries, then the energy associated with that strain gradient would be lost by ordinary elements. Therefore, Shu et al. introduced additional degrees of freedom (DOFs) at element nodes where strain components appeared as DOFs. However, this lead to a situation where the DOFs were not completely independent from each other and the equations became overdetermined. Hence, the error arising from these definitions was afterwards minimized using the Lagrange multiplier method.

Instead, the present investigation utilizes a method which converges precisely. In consequence, one obtains a global linear elastic stiffness-matrix which may be solved exactly. For this purpose an overlapping mesh technique will be defined.

2.1 Definition of Elements

First, 9 node quadrilateral elements consisting of isoparametric 4 node sub-elements are defined as depicted in Figure 1:

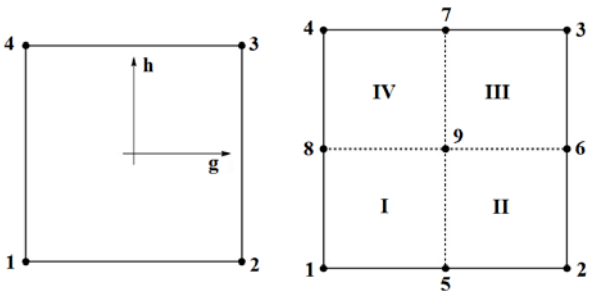

Figure 1: (a) left: Sub-elements are isoparametric four node quadrilaterals. (b) right: 9-node elements consist of four 4-node sub-elements.

The interpolation functions for the displacements on sub-element level read as [13, 14]

$$U = \tfrac{1}{4}(1-g)(1-h)U_1 + \tfrac{1}{4}(1+g)(1-h)U_2 + \tfrac{1}{4}(1+g)(1+h)U_3 + \tfrac{1}{4}(1-g)(1+h)U_4 \quad (4)$$

where g and h are the coordinates of the isoparametric space and U_1, U_2, U_3 and U_4 are the displacement vectors of the nodes 1, 2, 3, and 4, respectively. Square shaped elements of this type were already used in a preceding article [14], where a simpler version of strain gradient elasticity was introduced. The strains and the strain gradients η_{112}, η_{121}, η_{212} and η_{221} are evaluated at integration points in the middle of sub-elements through differentiation of interpolation functions in the element coordinate system. Thereafter, the remaining strain gradients η_{111}, η_{122}, η_{211} and η_{222} are calculated on element level by a difference method; i.e. the difference of strains in neighbouring sub-elements is divided through the distance of the integration points.

Next, the residual nodal forces have to be calculated as function of nodal displacements (see for instance reference [15]). One derives the nodal forces by superposition of stresses σ_{ij} and higher order stresses μ_{ijk}. The contribution of the stresses to nodal forces is obtained from the energy density according to

$$\sigma_{ij} = \frac{\partial w}{\partial \varepsilon_{ij}}, \qquad (5)$$

while higher order stresses are obtained from

$$\mu_{ijk} = \frac{\partial w}{\partial \eta_{ijk}}. \qquad (6)$$

The direction of nodal forces related to higher order stresses is obtained from the rule that some μ_{ijk} is always counteracting the deformation introduced by the corresponding η_{ijk}, as shown in Figures 2 to 4. Further, the residual nodal forces of the entire element must lead to static equilibrium so that neither translational nor rotational forces will remain.

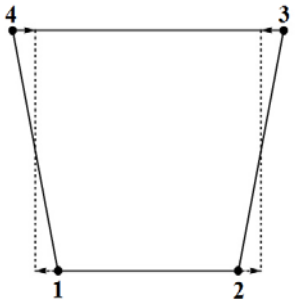

Figure 2: Direction of the residual nodal forces for the case of $\mu_{112} = \mu_{121}$, schematically. The higher order stresses are counteracting the deformation introduced by the corresponding strain gradients $\eta_{112} = \eta_{121}$.

The value of nodal forces is obtained from a principle of virtual work requiring that the work done by external nodal forces equals the elastic energy stored in the volume of the element.

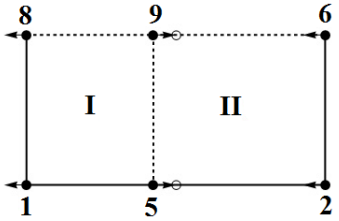

Figure 3: μ_{111} is here applied to the lower half of the entire element, schematically.

In the case of the higher order stresses μ_{111} it will in general make a difference whether η_{111} was calculated by comparison of sub-elements I and II as depicted in Figure 3, or from sub-elements III and IV. Therefore, μ_{111} is applied to the upper and lower half of the element separately. The higher order stresses μ_{122}, μ_{211}, and μ_{222} are treated in analogous style.

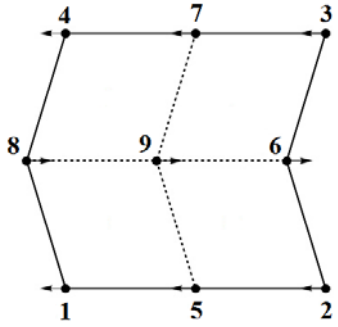

Figure 4: The higher order stress μ_{122} introduces residual nodal forces in the element, schematically.

Figure 4 demonstrates how higher order stresses μ_{122} are applied to the element. It is interesting to notice that forces on node 9 are present. This demonstrates that higher order stresses are more than just normal stresses and surface tractions along the outer borders of a volume element. Instead, higher order stresses may also act on the inside of volume elements. This behavior is a consequence of the fact that the tensor of higher order stresses has a different rank compared to ordinary stresses.

According to these rules the residual nodal forces of the 9 node elements are a unique function of the displacements and vice versa, provided that rigid body motion is suppressed by boundary conditions. The calculation of nodal forces was shown in detail for a somewhat simpler version of strain gradient elasticity in reference [14].

In addition to the 9 node elements explained here also 6 node elements consisting of 2 sub-elements are needed in order to mesh the periphery of the samples. The interpolation functions of these sub-elements are the same as for 9 node elements, and residual nodal forces are evaluated along the same principles. However, with a horizontal 6 node element one cannot evaluate η_{122} and η_{222}, while η_{111} and η_{211} are not accessible for vertical 6 node elements. But this will not disturb the investigation, because the corresponding higher order stresses are ending at the free sample surface anyway.

2.2 Overlapping Mesh Technique

In this section the problem of meshing large samples is solved. When the elements explained above were used together with ordinary mesh technique, then one would get unpleasant discontinuities of strains at the element boundaries, while the strain gradient inside the elements would be underestimated. On the other hand, the method described by Shu et al.

[4] using additional DOFs related to strain components is avoided here, because it does not converge precisely. Instead, a linear elastic stiffness matrix is constructed which may be solved by matrix inversion. For this purpose an overlapping mesh is generated as depicted in Figure 5, schematically:

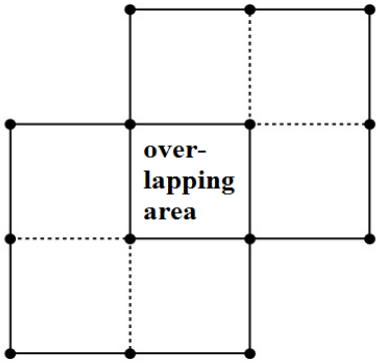

Figure 5: Two elements have one sub-element in common, which is located in the overlapping area.

According to this method the whole sample is covered twice with elements. Two neighbouring elements always have one sub-element in common. Thereby, the elements of the overlapping area are attached to the same nodes. At the periphery of the sample 6 node elements are used in order to fill up vacant spaces. In conclusion, the overlapping mesh technique results in a material stiffness which is twice as high as initially intended. But this was compensated by using halved values for Young's modulus and bending moduli at the element level.

3 Example: Shear Test

In order to demonstrate the advantages of the present approach, a shear test is simulated. Indeed, shear tests are widely used in engineering science, for instance for measuring the strength of adhesives or solder joints. However, the shear stresses are in general non-uniformly distributed over the specimen. According to simulations in the frame of classical continuum mechanics one even gets stress singularities which cannot easily be interpreted.

In this example a somewhat simplified shear test is performed in two dimensions, where a testing material is sheared between two pieces of rigid base material. By mesh refinement one can show that the FEM solution of classical continuum mechanics does not converge, whereas the simulation using strain gradient theory converges nicely against a finite value. The setup of the shear test is depicted in Figure 6, schematically. The material under test is here simulated using isotropic elasticity. The simulations were carried out with ABAQUS, whereby strain gradient effects were implemented through user subroutine UEL. The simulations were all done in the plane strain approximation.

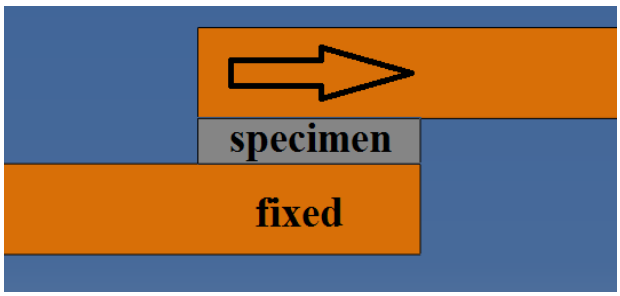

Figure 6: Setup of the shear test, schematically. The specimen connects two pieces, which are modelled as rigid bodies.

The aspect ratio of length to height of the tested specimen was 5:1, as may be seen in Figure 6. Further, a Young's modulus of 48 GPa and a Poisson ratio of 0.4 were assumed for the specimen. In all of the simulations shown hereafter the force acting on the upper sample holder was adjusted to receive an average shear stress of 1 MPa in the classical FEM simulations.

Realistic values for the bending moduli are not easy to obtain. But since they have the dimension of a force, the bending stiffness causes a size effect where strain gradient effects get more pronounced at smaller length scales. It is therefore possible to relate the value of bending moduli to the length scale of the experiment: Let l be the length of the specimen in horizontal direction. Then the bending moduli in [N] assumed in our simulation were $B_1 = B_2 = B_3 = B_4 = B_5 = 100 \cdot l^2$, where l has to be inserted in [mm]. Thereby, the values for the bending moduli were adjusted in order to see an onset of the size effect for the mechanical properties. In conclusion, the estimated value of l should be somewhere in the sub-millimeter range.

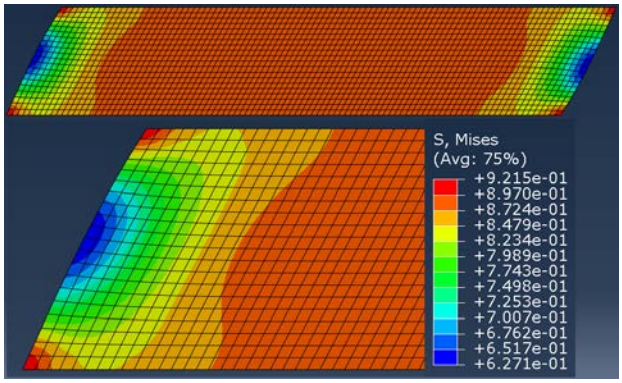

Figure 7: Plot of the von Mises stress [MPa] for the solution of strain gradient elasticity. A coarse mesh with 2121 nodes is shown. Top: entire sample. Bottom: magnification of left part of the sample.

The results derived on the basis of these assumptions are depicted in Figures 7, 8 and 9. Only the deformable sample was simulated in detail, while the rigid base material was considered in the boundary conditions. The Figures show plots for the von Mises stress, whereby the mesh size was refined during consecutive simulations. For comparison, Figures 10, 11 and 12 show the corresponding results derived from classical FEM simulations. The crucial question is whether convergence is achieved during mesh refinement.

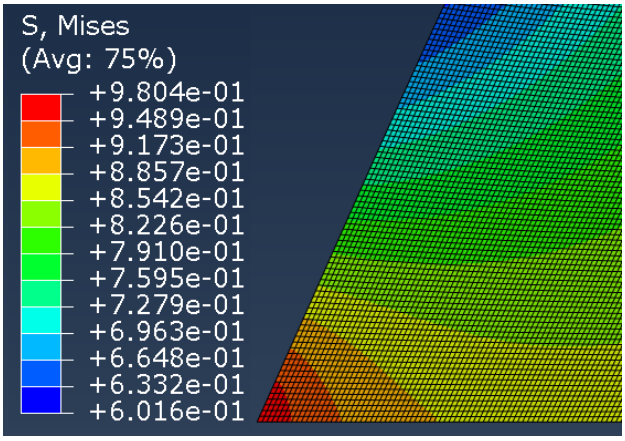

Figure 8: Plot of the von Mises stress [MPa] after reducing the sides of elements by a factor of 10 in comparison to Figure 7. The location of a stress concentration is shown in magnification.

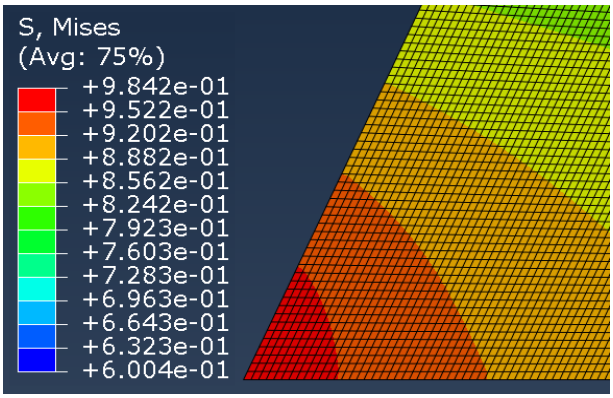

Figure 9: Plot of the von Mises stress [MPa]. The sides of elements were reduced by a factor of 2 compared to Figure 8. Thereby, the colour contours have changed very little compared to the previous Figure.

A comparison of Figures 8 and 9 shows that at this level a reduction of mesh size by a factor of 2 changes the results only marginally. In particular, the stress maximum increases very little.

On the other hand, Figures 10, 11 and 12 show how the results of FEM simulations according to classical continuum theory change during mesh refinement. Here, the maximum of stress increases significantly, because the stress concentration has the features of a stress singularity. Therefore, convergence cannot be achieved.

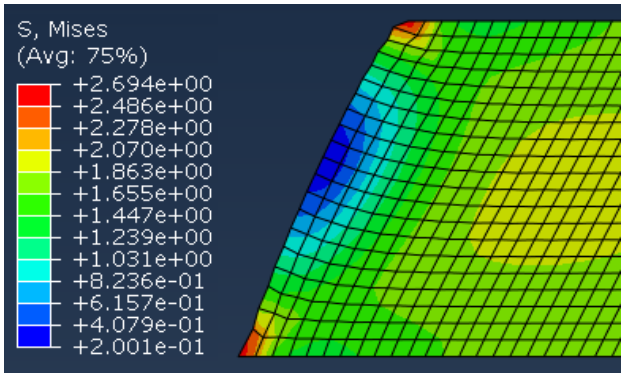

Figure 10: Plot of the von Mises stress [MPa] for the solution of classical continuum mechanics. The mesh size corresponds to that of Figure 7; i.e. the models have the same number of nodes.

The comparison of Figures 7 and 10 shows that hour-glassing and spurious modes are well suppressed in strain gradient elasticity, while these problems become quite apparent using element type CPE4R in ABAQUS.

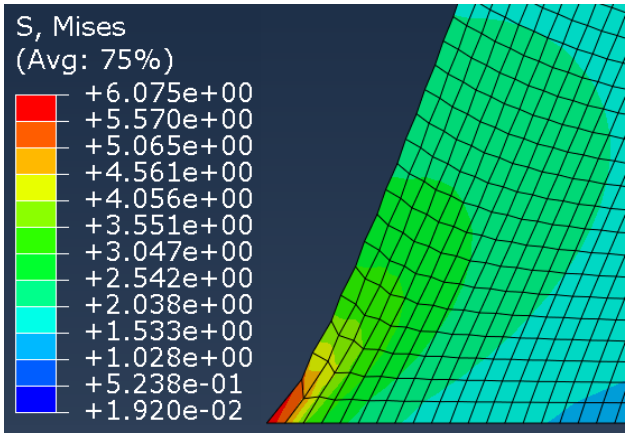

Figure 11: Plot of von Mises stress [MPa] for classical continuum theory using the same mesh size as in Fig. 8.

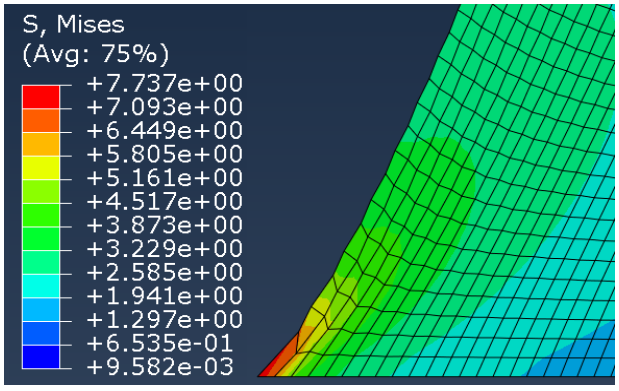

Figure 12: Plot of the von Mises stress [MPa] for the same mesh size as in Figure 9. We see the typical characteristics of a stress singularity.

It should also be noticed here that the stress values of strain gradient elasticity are on the average somewhat lower than in classical continuum mechanics, because the higher order stresses also carry a part of the external load.

4 Discussion

In the preceding section it was demonstrated how the Finite Element solution of strain gradient elasticity converged for a shear test. However, a single example is not sufficient to validate the method in general. Therefore, in this section the reasons are summarized which lead to the conclusion that the approximations of the present approach will always converge:

The FEM simulation of strain gradient elasticity may be viewed as the solution of a variational calculation. In order to derive the equilibrium condition, the internal energy of the model is minimized. The whole simulation is linear, and the stiffness matrix is symmetric as required by a theorem of Maxwell [16]. Consequently, the relation between nodal forces and displacements reads as $F = K \cdot U$. Further, the stiffness matrix K is positive definite. This means that any deformation results in an increase of internal energy compared to the undeformed state. In consequence, spurious modes like hour-glassing do not exist here. Any configuration of the model leads to a unique vector of nodal forces and vice versa. Therefore, any discrete model formulated within this version of strain gradient elasticity will certainly converge in the sense that residual forces between neighbouring elements disappear.

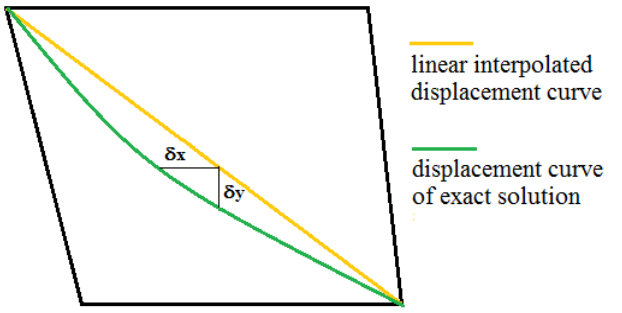

Figure 13: Distorted mesh, linear interpolation function and exact displacement curve, schematically.

Next, the model behaviour during mesh refinement is discussed. Let us here for the moment assume that the displacement field u(x) of the exact solution shall at least be three times differentiable, and the absolute value of all derivatives shall have an upper bound. Let us further assume that the displacements at the nodes of the deformed mesh are perfectly matching the displacement field. Then the deviations δx and δy between interpolated displacement curve and exact solution at the integration points, as depicted in Figure 13, are a measure for the quality of the approximation. If the values of δx and δy converge against zero during mesh refinement, then stresses and strains will converge as well. However, the convergence of δx and δy against zero during mesh refinement is obvious, because the curvature of the exact solution is limited according to our assumptions. The linear interpolation functions of the sub-elements are approximating the exact displacement curve by polygonal lines, and if the element size gets continuously smaller, then δx and δy will eventually approach zero. An equivalent statement is true for the numerical error of strain gradients obtained by the difference method. The comparison of neighbouring sub-elements results in correct average values for strain gradients, and the maximum deviation from the average is limited by the second gradient of strains and the element size. In conclusion, strains and strain gradients will converge against the exact solution during mesh refinement. This automatically implies convergence of the internal energy.

So far, it was just assumed that strains and strain gradients have an upper bound. Or to put it in other words, it was shown that the simulations converge if the exact solution of the model has no stress singularities. However, it is possible to enhance this statement: The stress singularities at sharp edges, at cracks or at material transitions, which are common in classical continuum theory, are all disappearing in the present version of strain gradient elasticity. In the vicinity of a hypothetical stress singularity, higher order stresses would become extremely strong so that the singularity would be suppressed there: Let for instance f'(x) have a singularity at x_0. Then f''(x) will become singular there as well, and close to x_0 f'' will exceed f' by far. Indeed, even f''/f' will become singular at x_0. But in the present approach higher order stresses are always counteracting singularities of stress, since the bending stiffness tries to distribute the load uniformly over the sample. In conclusion, within the theory proposed here such a hypothetical singularity cannot exist at sharp edges, cracks or material transitions.

5 Summary and Conclusions

In the present study, the theory of strain gradient elasticity, which was first proposed by Toupin [5, 6]

and Mindlin [1, 3], has been reformulated. Instead of using an asymmetric stress, a symmetric stress tensor was used throughout the model calculations. In this way invariance of the theory with respect to rotations of the coordinate system was achieved. Further, the theory was implemented in the commercial Finite Element code ABAQUS through user subroutine UEL. In order to demonstrate the convergence of this approach, the subroutine was applied to a theoretical shear test. Finally, the convergence statement was generalized on the grounds of theoretical considerations.

References:

[1] Mindlin, R. D., Influence of couple-stresses on stress concentrations, *Experimental Mechanics* Vol. 3, 1963, pp. 1-7.

[2] Cosserat, E., Cosserat, F., *Théorie des corps dé formables*, Librairie Scientifique A. Hermann et Fils, Paris. 1909 (English translation by Delphenich, D., 2007. *Theory of deformable bodies*.)

[3] Mindlin, R. D., Micro-structure in linear elasticity, *Arch. Rat. Mech. Anal.* Vol. 16, 1964, pp. 51-78

[4] Shu, J. Y., King, W. E., Fleck, N. A., Finite elements for materials with strain gradient effects, *Int. J. Numer. Meth. Engng.*, Vol. 44, 1999, pp. 373-391.

[5] Toupin, R., Elastic materials with couple-stresses, *Arch. Rat. Mech. Anal.* Vol. 11, 1962, pp. 385-414

[6] Toupin, R., Theories of elasticity with couple-stresses, *Arch. Rat. Mech. Anal.* Vol. 17, 1964, pp. 85-112

[7] Mindlin, R. D., Tiersten, H., Effects of couple-stresses in linear elasticity, *Arch. Rat. Mech. Anal.* Vol. 11, 1962, pp. 415-448

[8] Mindlin, R. D., Eshel, N., On first strain-gradient theories in linear elasticity, *Int. J. Solids and Struct.* Vol. 4, 1968, pp. 109-124

[9] Fleck, N. A., Hutchinson, J. W., A phenomenological theory of strain gradient effects in plasticity, *J. Mech, Phys. Solids* Vol. 41 (12)1993, pp. 1825-1857

[10] Fleck, N. A., Hutchinson, J. W., Strain Gradient Plasticity, *Advances in Applied Mechanics* Vol. 33, 1997, pp. 295-362

[11] Lam, D. C. C., Yang, F., Chong, A. C. M., Wang, J., Tong, P., Experiments and theory in strain gradient elasticity, *J. Mech. Phys. Solids* Vol. 51, 2003, pp. 1477-1508

[12] Zybell, L., Mühlich, U., Kuna, M., Zhang, Z. L., A three dimensional finite element for gradient elasticity based on a mixed-type formulation, *Computational Materials Science* Vol. 52, 2012, pp. 268-273

[13] Bathe, K.-J., *Finite Element Procedures*, Prentice Hall, Pearson Education Inc., 2006

[14] Lederer, M., Magnien, J., Khatibi, G. Weiss, B., FEM simulation of the size and constraining effect in lead-free solder joints with the theory of strain gradient elasticity. IOP conference series **602**, 2015, 12020

[15] ABAQUS 6.10 User Subroutine Reference Manual, Simulia, Dassault Systems, 2010

[16] Hartmann, F., *Green's Functions and Finite Elements*, Springer, 2012.